Thermodynamic Analysis Shows Conformational Coupling and Dynamics Confer Substrate Specificity in Fructose-1,6-bisphosphate Aldolase†

John A. Pezza,‡,§ Jack D. Stopa,‡ Elizabeth M. Brunyak,‡ Karen N. Allen,*,|| and Dean R. Tolan*,‡

Department of Biology, Boston University, 5 Cummington Street, Boston, Massachusetts 02215, and Department of Physiology and Biophysics, Boston University School of Medicine, 715 Albany Street, Boston, Massachusetts 02118-2394

Received April 16, 2007; Revised Manuscript Received September 4, 2007

ABSTRACT: Conformational flexibility is emerging as a central theme in enzyme catalysis. Thus, identifying and characterizing enzyme dynamics are critical for understanding catalytic mechanisms. Herein, coupling analysis, which uses thermodynamic analysis to assess cooperativity and coupling between distal regions on an enzyme, is used to interrogate substrate specificity among fructose-1,6-(bis)phosphate aldolase (aldolase) isozymes. Aldolase exists as three isozymes, A, B, and C, distinguished by their unique substrate preferences despite the fact that the structures of the active sites of the three isozymes are nearly identical. While conformational flexibility has been observed in aldolase A, its function in the catalytic reaction of aldolase has not been demonstrated. To explore the role of conformational dynamics in substrate specificity, those residues associated with isozyme specificity (ISRs) were swapped and the resulting chimeras were subjected to steady-state kinetics. Thermodynamic analyses suggest cooperativity between a terminal surface patch (TSP) and a distal surface patch (DSP) of ISRs that are separated by >8.9 Å. Notably, the coupling energy (ΔG_I) is anticorrelated with respect to the two substrates, fructose 1,6-bisphosphate and fructose 1-phosphate. The difference in coupling energy with respect to these two substrates accounts for ~70% of the energy difference for the ratio of k_{cat}/K_m for the two substrates between aldolase A and aldolase B. These nonadditive mutational effects between the TSP and DSP provide functional evidence that coupling interactions arising from conformational flexibility during catalysis are a major determinant of substrate specificity.

Recent evidence shows dynamic fluctuations of structure are essential components of enzyme catalysis (*1*). While it is likely that most enzymes exhibit flexibility as part of the catalytic process, the role of this movement is enzyme-specific. For example, in the case of dihydrofolate reductase (DHFR), backbone and side chain motions are essential for cofactor binding, substrate binding, and catalysis (*2*). Thus, identifying and characterizing these motions are paramount to understanding enzyme mechanisms.

Recently, the importance of conformational flexibility has been highlighted in the study of ligand binding and catalysis, as inferred from X-ray crystallographic and NMR structures as well as computational analysis. The term "allostery" has been applied to the transmission of energy resulting from structural rearrangement and/or dynamic changes within a single-domain protein (*3*−*5*). In addition to structural and computational data, evolutionary data for a protein family have been used to show that conserved sets of interacting residues form connected pathways through the protein to transmit changes upon ligand binding (*6*). Not only ligand binding but also catalysis is dependent upon the inherent mobility of a protein during the catalytic cycle with one or more of the catalytic steps being reflected in an intrinsic motion of the enzyme (for a review, see ref *1*, and for a recent example, see ref *7*). Thus, the innate mobility of the protein scaffold is manifested in the various steps of the catalytic cycle. Indeed, extensive studies of hydrogen transfer in proteins are consistent with the concept that protein dynamics create transient heavy-atom configurations with a favorable electrostatic environment for proton and hydride transfer (*1*, *8*−*12*). In comparison, determining how conformational flexibility affords the remarkable selectivity of enzymes has received less attention. However, recent work on T7-DNA polymerase has invoked a role for enzyme dynamics in distinguishing correct nucleotide incorporation from misincorporation (*13*).

Here, multiple mutational analyses in fructose-1,6-(bis)-phosphate aldolase (aldolase, EC 4.1.2.13) are used to identify and characterize conformational coupling as a potential mechanism conferring substrate specificity among aldolase isozymes. Aldolase catalyzes the reversible C−C bond cleavage of fructose 1,6-(bis)phosphate (Fru 1,6-P_2)[1] and fructose 1-phosphate (Fru 1-P) in its roles in glycolysis, gluconeogenesis, and fructose metabolism (*14*). Aldolase

† This work was supported by Grant GM60616 (to D.R.T. and K.N.A.), Grant DK065089 (to D.R.T.), and Training Grant HL07291 (to J.A.P.) from the National Institutes of Health.

* To whom correspondence should be addressed. D.R.T.: Department of Biology, 5 Cummington St., Boston, MA 02215; phone, (617) 353-5310; fax, (617) 358-0338; e-mail, tolan@bu.edu. K.N.A.: Department of Physiology and Biophysics, 715 Albany St., Boston University School of Medicine, Boston, MA 02118; phone, (617) 638−4398; fax, (617) 638−4273; e-mail, allen@med-xtal.bu.edu.

‡ Boston University.

§ Present address: Department of Molecular Biology, Cell Biology and Biochemistry, Brown University, 185 Meeting St., Box G-L2, Providence, RI 02912.

|| Boston University School of Medicine.

10.1021/bi700713s CCC: $37.00
Published on Web 10/13/2007

isozymes are distinguished by their unique expression profiles and substrate specificities (*15*). Aldolase A is expressed primarily in skeletal muscle and has the highest rate of turnover toward Fru 1,6-P_2 of the three isozymes (*15*−*17*). Aldolase B is expressed primarily in liver and kidney where most Fru 1-P degradation takes place (*14*, *18*). While the catalytic mechanism of aldolase is well-characterized (*19*−*21*) and crystal structures of all three human isozymes have been determined (*22*−*24*), it is still unclear how aldolase catalyzes the cleavage of the two substrates with distinct and physiologically relevant efficiencies. For example, consistent with its role in gluconeogenesis, aldolase B has equal turnover numbers for the two hexose substrates and has a lower K_m value for glyceraldehyde 3-phosphate and dihydroxyacetone phosphate than aldolase A (*17*). Correspondingly, aldolase A has evolved to cleave Fru 1,6-P_2 more efficiently than Fru 1-P (as evidenced by the k_{cat}/K_m ratio for Fru 1,6-P_2 to Fru 1-P of 70000). This ratio for aldolase B is ∼900; therefore, the evolution of these parameters for aldolase A compared to that of aldolase B has resulted in an ∼80-fold (70000/900) difference in selectivity between the two hexoses.

Previous work attempting to decipher the root of isozyme specificity has identified a set of residues conserved among, but not between, each isozyme, termed isozyme-specific residues (ISRs). Surprisingly, ISRs are not located at or near the active site but mostly (24 of 27) fall on the surface of the protein (*25*). Moreover, a large proportion of ISRs are found in the C-terminal region (CTR) of the enzyme. The role of ISRs was previously examined by swapping ISRs from aldolase B into aldolase A, demonstrating that the ISRs are necessary and sufficient to confer kinetic parameters (k_{cat} and K_m) of aldolase B onto aldolase A (*25*). Because of their conservation and involvement in conferring substrate specificity, it is hypothesized that interactions between ISRs are responsible for altering the structure of the active site from a distance.

One means by which enzymes may confer substrate specificity at a distance would involve dynamic cooperation and coupling among sets of ISRs. Herein, multiple mutational analyses are employed as a novel method to attribute the role of conformational coupling to substrate specificity among aldolase isozymes. Traditionally, this analysis is performed by making two separate, single-residue mutations and the corresponding double mutation, calculating the change in free energy ($\Delta\Delta G$) associated with these changes, and comparing the change in free energy with that of the double mutant (*9*, *26*, *27*). If the changes in free energy of the two single mutants do not sum to the change in free energy for the double mutant, then a cooperative and/or coupling mechanism between the residues is invoked. To perform the analogous experiment for aldolase ISRs, groups of mutations were analyzed rather than single amino acid substitutions. Multiple mutational analyses revealed that substrate specificity of aldolase A was conferred by cooperative effects between two distantly located surface patches, one of which includes the CTR. This analysis exposes a means by which these cooperative effects among ISRs affect substrate specificity in enzymes with seemingly identical active sites.

[1] Abbreviations: ISR, isozyme-specific residue; Fru 1,6-P_2, fructose 1,6-bisphosphate; Fru 1-P, fructose 1-phosphate; CTR, C-terminal region; TSP, terminal surface patch; DSP, distal surface patch; DTNB, 5,5′-dithiobis(2-nitrobenzoic acid).

Table 1: Site-Directed Mutagenesis

enzyme[a]	amino acid substitutions
AB_P	S38T, I39M, A40G, S45R, Q60E, P71Q, R91K, G102I, K311A, L320K, S353T, E354Q, I358T, S359A, H361Y
AB_NP	Y58F, V113A, H156Q, I182L, P262A, A296K, Y327F
AB_TSP	S38T, I39M, A40G, S45R, K311A, S353T, E354Q, I358T, S359A, H361Y
AB_DSP	Q60E, P71Q, R91K, G102I, L320K
AB_NPS	V113A, H156Q, P262A, A296K
AB_NPB	Y58F, I182L, Y327F

[a] P, patch; NP, nonpatch; TSP, terminal surface patch; DSP, distal surface patch; NPS, nonpatch surface; NPB, nonpatch buried.

MATERIALS AND METHODS

Materials. Restriction endonucleases, T4 DNA ligase, $Vent_R$ DNA polymerase, and ThermoPol buffer were from New England Biolabs. AmpliTaq DNA polymerase was from Applied Biosystems. Glycerol-3-phosphate dehydrogenase and triosephosphate isomerase were from Roche Applied Science. Deoxynucleoside triphosphates and CM-Sepharose CL-6B were from Amersham Biosciences. Oligonucleotides used for site-directed mutagenesis and sequencing were from Midland Certified Reagent Company, Inc. All other chemicals were from Sigma-Aldrich Chemical Co.

Site-Directed Mutagenesis. All mutant aldolases were generated via multiple site-directed mutagenesis using overlapping oligonucleotides (*28*). Unless otherwise stated, all oligonucleotides complement pPB14, which expresses rabbit aldolase A (*29*). Oligonucleotide sequences are provided as Supporting Information.

Full-length cassettes were subcloned into *Eco*RI and *Hin*dIII sites in pPB1 (*30*). The different expression constructs are described in Table 1. The expression plasmid, pAB_DSP, was constructed with the following oligonucleotides: geneU, AB_DSP1, AB_DSP2, AB_DSP3, AB_DSP4, AB_DSP5, AB_DSP6, and geneL. The expression plasmid, pAB_TSP, was generated in two steps. First, the pAB_Cterm plasmid was constructed with the following oligonucleotides: geneU, ABC1, ABC2, and geneL. Second, pAB_Cterm was used as a template for the following oligonucleotides to generate pAB_TSP: geneU, ABD1, ABD2, AB_TSP3, AB_TSP4, AB_TSP5, AB_TSP6, and geneL. The expression plasmid, pAB_P, was also generated in two steps. First, the pInt plasmid was created by splicing together the 474 bp fragment generated by cutting pAB_TSP with *Nco*I and *Hin*dIII into the 3402 bp fragment of pAB_DSP, cut with the same enzymes. Second, pInt was used as a template for the following oligonucleotides to generate pAB_P: geneU, ABD1, ABD2, AB_DSP5, AB_DSP6, and geneL. The expression plasmid, pAB_NP, was constructed with the following oligonucleotides: geneU, AB_NP1, AB_NP2, AB_NP3, AB_NP4, AB_All5, AB_All6, 5′−3′ (forward); AB_All7, AB_All8, AB_NP5, AB_NP6, ABD9, ABD10, AB_NP7, AB_NP8, and geneL. The expression plasmid, pAB_NPS, was constructed with the following oligonucleotides: geneU, AB_NP3, AB_NP4, AB_All5, AB_All6, AB_NP5, AB_NP6, ABD9, ABD10, and AB_NP7. The pAB_NPS full-length PCR product was subcloned into

pPB14 at the *Eco*RI and *Eag*I sites. The expression plasmid, pAB_NPB, was constructed with the following oligonucleotides: geneU, AB_NP1, AB_NP2, AB_All7, AB_All8, AB_NP7, AB_NP8, and geneL. The expression plasmid, pAld337, was constructed in two steps. First, the oligonucleotides U1nde and L337sap, complementing pPB14, were used to generate a PCR fragment corresponding to the first 337 amino acids of rabbit aldolase A. The engineered restriction sites *Nde*I and *Sap*I were used for in-frame subcloning in the *Sce*VMA intein/chitin binding domain from pTYB1 (New England Biolabs). The construct encoding an aldolase with only two Cys residues, gBi, used a 207 bp *Bst*EII−*Eag*I fragment from pGTET, which has all surface Cys residues (72, 239, 289, and 338) substituted with Ala (*31*), ligated pPB14. The 207 bp fragment encodes the C239A and C289A substitutions of pGTET. All fragments were amplified as previously described (*25*), and resulting clones were screened by DNA sequence determination (Boston University Core Sequencing Facility).

Expression and Purification of Recombinant Aldolases. Expression and purification of substituted aldolases were performed as described previously (*29*). Briefly, purification used affinity elution from CM-Sepharose CL-6B with 2.5 mM Fru 1,6-P_2 at pH 8.3 for AB_NP, AB_P, AB_NPS, AB_NPB, AB_TSP, AB_DSP, and gBi. The truncated form of aldolase, Ald337, was purified using the IMPACT-CN protein purification system as previously described (*32*).

Characterization of Chimeric Aldolases. Aldolase activity toward Fru 1,6-P_2 and Fru 1-P was measured as described previously (*29*, *33*). Briefly, a decrease in A_{340} was measured from an assay coupled to β-NADH oxidation by glycerol-3-phosphate dehydrogenase. Enzymes were diluted in 50 mM TEA-HCl (pH 7.4), 10 mM EDTA, 20 μg/mL glycerol-3-phosphate dehydrogenase, triosephosphate isomerase, and 0.2 mM β-NADH. For the AB_P chimera, the Fru 1,6-P_2 concentration ranged from 0.6 to 6.0 μM with 2 μg/mL enzyme and the Fru 1-P concentration ranged from 1100 to 8000 μM with 4 μg/mL enzyme. For chimeras AB_NP, AB_NPS, and AB_NPB, the Fru 1,6-P_2 concentration ranged from 3.0 to 100 μM with 0.5 μg/mL enzyme and the Fru 1-P concentration ranged from 2500 to 80000 μM with 100 μg/mL enzyme. For the AB_TSP chimera, the Fru 1,6-P_2 concentration ranged from 4.5 to 35 μM with 1.1 μg/mL enzyme and the Fru 1-P concentration ranged from 5000 to 60000 μM with 10 μg/mL enzyme. For the AB_DSP chimera, the Fru 1,6-P_2 concentration ranged from 5.0 to 80 μM with 0.5 μg/mL enzyme and the Fru 1-P concentration ranged from 5000 to 60000 μM with 10 μg/mL enzyme. For the Ald337 chimera, the Fru 1,6-P_2 concentration ranged from 20 to 600 μM with 18 μg/mL enzyme and the Fru 1-P concentration ranged from 2500 to 80000 μM with 70 μg/mL enzyme. For gBi, the Fru 1,6-P_2 concentration ranged from 6 to 200 μM with 1.3 μg/mL enzyme. Assays were performed at 30 °C in triplicate using a SpectroMAX 190 spectrophotometer (Molecular Devices, Inc.) in a final volume of 350 μL.

Inactivation of Aldolase by Oxidation. Oxidation was performed as described previously (*34*) except for changes in concentration. The oxidants were *o*-phenanthroline (60 μM) and cupric sulfate (20 μM). Concentrations of Fru 1,6-P_2 and Fru 1-P were 5K_m (0.05 and 200 mM, respectively). Briefly, aldolases (1 mg/mL) in 100 mM Tris-HCl (pH 8.4) were incubated with oxidants in the presence or absence of substrate. At various times, aliquots (10 μg) were removed, diluted 100-fold, and assayed for activity at 25 °C. The presence of unoxidized thiols was determined by reaction of 90 μg aliquots of aldolase with 3 mM 5,5′-dithiobis(2-nitrobenzoic acid) (DTNB) in 100 mM Tris (pH 9.4) (*34*). Absorbance was measured at 412 nm after 5 min at 25 °C.

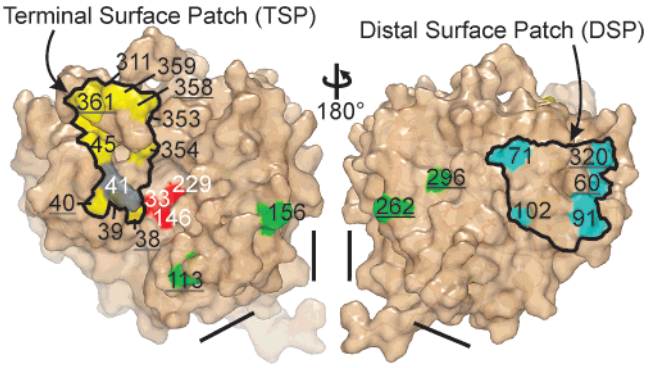

FIGURE 1: Location of aldolase A and B ISRs on the aldolase monomer. A surface model of the aldolase A monomer (PDB entry 1ADO) showing the location of aldolase A and B (residue number underlined) ISRs with respect to the active site (two views shown, 180° rotation about the *y* axis). ISRs of TSP (yellow), ISRs of the DSP (cyan), and nonpatch surface ISRs (green) are labeled, and the patches are outlined. Active site residues are colored red, and residue 41, involved in binding the C6-phosphate, is colored gray. The approximate locations of tetramer interfaces are indicated with black bars. This figure was created using PyMOL version 0.97 (*58*).

RESULTS

Spatial Analysis of ISRs. Isozyme-specific residues (ISRs) that confer the kinetic properties of the aldolase isozymes have previously been identified (*25*). Here, ISRs were further analyzed on the basis of their location in the three-dimensional structure (Figure 1). Of the 23 ISRs in aldolase A and aldolase B, 16 cluster into two surface patches, the terminal surface patch (TSP) and the distal surface patch (DSP), hereafter termed "patch" ISRs, and the remaining seven residues are termed "nonpatch" ISRs. Nonpatch ISRs were categorized on the basis of their exposure to solvent. Four of the seven nonpatch ISRs were solvent accessible as determined from a Connolly surface map (*35*), while the remaining three residues were buried (residues 58, 182, and 327).

To determine if potential coupling interactions among these conserved groups of residues confers the differential kinetics between isozymes, chimeric enzymes were created by swapping each subset of ISRs (Table 1). Swapping ISRs was performed by incorporating aldolase B ISRs into aldolase A while replacing aldolase A ISRs with the corresponding aldolase B residue. The location of these substitutions in the primary sequence is shown in Figure 2. The resulting chimeric proteins were expressed in *Escherichia coli* and purified to >95% as assayed by SDS−PAGE.

Steady-State Kinetics. All chimeras were characterized via steady-state kinetics with the substrates Fru 1,6-P_2 and Fru 1-P (Table 2). It is known that the rate-limiting step for wild-type aldolases is product release (*20*, *36*), and since the chimeras are fully active enzymes, the rate-limiting step is not likely changed for the chimeras. If so, K_m would be defined identically for all enzymes. The chimera in which

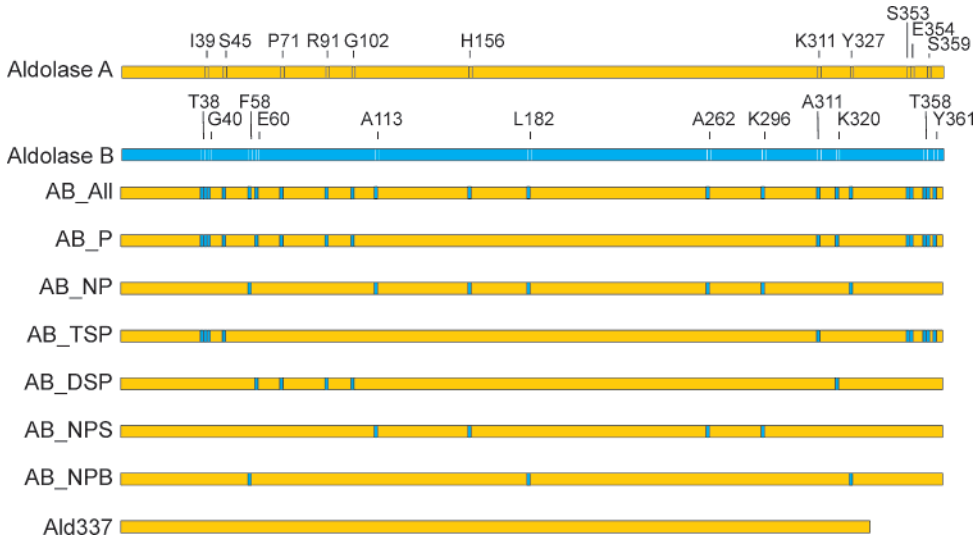

FIGURE 2: Diagrammatic representation of aldolase chimeras. Wild-type aldolases A and B, 363 amino acid residues each, are represented as yellow and blue boxes, respectively, above which the ISRs are indicated. The ISRs engineered in each chimera are similarly indicated in color.

Table 2: Steady-State Kinetics of Aldolase Chimeras

	Fru 1,6-P_2		Fru 1-P	
	k_{cat} (s^{-1})	K_m (μM)	k_{cat} (s^{-1})	K_m (μM)
aldolase A[a]	10.2 ± 0.4	9.5 ± 0.9	0.63 ± 0.02	40000 ± 2000
aldolase B[a]	1.5 ± 0.1	0.84 ± 0.05	1.4 ± 0.1	720 ± 40
AB_All[a]	1.07 ± 0.07	1.1 ± 0.1	1.47 ± 0.08	2600 ± 200
AB_P	2.4 ± 0.2	5.1 ± 0.4	1.3 ± 0.1	3300 ± 300
AB_NP	7.6 ± 0.4	4.0 ± 0.4	1.6 ± 0.1	47000 ± 3000
AB_TSP	1.3 ± 0.1	7.1 ± 0.4	1.2 ± 0.1	9400 ± 1000
AB_DSP	7.2 ± 0.4	8.5 ± 0.4	2.0 ± 0.1	8100 ± 600
AB_NPS	8.7 ± 0.5	6.0 ± 0.3	1.9 ± 0.1	71000 ± 4000
AB_NPB	9.7 ± 0.5	6.8 ± 0.3	2.2 ± 0.1	85000 ± 4000
Ald337	0.097 ± 0.006	200 ± 10	0.017 ± 0.001	2200 ± 100

[a] Data from ref *25*.

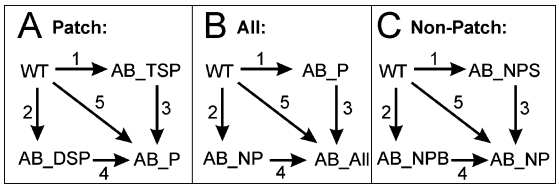

FIGURE 3: Thermodynamic cycles among aldolase chimeras. For each cycle, arrows 1 and 4 indicate the substitution of one set of ISRs, while arrows 2 and 3 indicate the substitution of the other set of ISRs. The diagonal arrow 5 indicates the double substitution. (A) ISRs involved in the "Patch" (TSP and DSP) cycle. (B) ISRs involved in AB_All (*25*) ("All") made with patch (P) and nonpatch (NP) residues. (C) ISRs involved in the "Non-patch" cycle made with buried (NPB) and surface (NPS) residues.

all ISRs had been swapped from aldolase B into aldolase A (AB_All) exhibits k_{cat} and K_m parameters indistinguishable from those of aldolase B (*25*). Compared to that of AB_All, the loss of nonpatch residues in AB_P resulted in a 5-fold increase in K_m toward Fru 1,6-P_2, making it more similar to aldolase A than aldolase B (Table 2). However, the turnover number was very similar to that of aldolase B. Toward the substrate Fru 1-P, AB_P displayed K_m and k_{cat} values more similar to those of aldolase B than to those of aldolase A. In a complementary experiment, the contribution of nonpatch ISRs alone was analyzed with the construct AB_NP, which exhibited kinetic parameters toward Fru 1,6-P_2 and Fru 1-P more similar to those of aldolase A than to those of aldolase B. The possible exception was the k_{cat} toward Fru 1-P, which was similar to that of aldolase B. Overall, the results are consistent with an effect on K_m toward Fru 1,6-P_2 associated with the combined presence of patch and nonpatch residues.

Similarly, the involvement of the two patches of AB_P in substrate specificity was analyzed using the chimeras AB_TSP and AB_DSP. The kinetic profile of AB_TSP toward Fru 1-P showed that the k_{cat} was similar to that of aldolase B (Table 2). The K_m value was decreased by 5-fold compared to that of aldolase A, making it intermediate between the values for A and B. Remarkably, toward Fru 1,6-P_2, AB_TSP had a K_m value more similar to that of aldolase A yet attained a k_{cat} indistinguishable from that of aldolase B. As for AB_DSP, steady-state kinetic analysis toward Fru 1-P revealed activities similar to those of AB_TSP, whereas the kinetic parameters toward Fru 1,6-P_2 were indistinguishable from those of aldolase A.

Similar analysis of the chimeras that separate the surface and buried nonpatch ISRs using AB_NPS and AB_NPB showed that they were similar to each other and each demonstrated the same kinetic differences from wild-type aldolase A as did the combination of the two (AB_NP) (Table 2). Thus, dividing the nonpatch residues into buried and surface residues did not dissect function. In addition, comparison of all nonpatch chimeras (AB_NP, AB_NPS, and AB_NPB) relative to aldolases A and B showed that the role of these residues in distinguishing kinetic parameters was relatively minor. The fact that the k_{cat} value toward Fru 1-P increased >2-fold for most chimeras relative to that of aldolase A demonstrated that all these enzymes were not simply impaired in function.

Nonadditive Mutational Effects in Aldolase. Interaction energies between two substitution sites can be assessed by summing the change in energy associated with each substitution and comparing this sum to the change in energy associated with the double substitution (*9*, *26*, *27*). This approach was applied to the ISR subsets; the subsets of ISRs represent a single substitution, and a combination of these subsets represents the double substitution. Three thermodynamic cycles among such aldolase chimeras were analyzed (Figure 3). First, the change in free energy associated with

Table 3: Comparison of Free Energy Differences among Chimeras toward Fru 1,6-P_2[a]

thermodynamic cycle		$\Delta\Delta G^{\ddagger}$ (kcal/mol) individual chimeras		sum	combined chimeras	ΔG_I (kcal/mol)
		AB_TSP	AB_DSP		AB_P	
Patch	k_{cat}	1.2 ± 0.2	0.21 ± 0.04	1.4 ± 0.2	0.9 ± 0.2	−0.6 ± 0.2
	K_m	0.18 ± 0.04	0.07 ± 0.02	0.24 ± 0.04	0.4 ± 0.1	0.1 ± 0.1
	k_{cat}/K_m	1.0 ± 0.2	0.14 ± 0.04	1.2 ± 0.2	0.5 ± 0.2	−0.7 ± 0.4
		AB_P	AB_NP		AB_All	
All	k_{cat}	0.9 ± 0.2	0.17 ± 0.02	1.0 ± 0.2	1.3 ± 0.2	0.3 ± 0.4
	K_m	0.4 ± 0.1	0.5 ± 0.1	0.9 ± 0.2	1.3 ± 0.4	0.4 ± 0.4
	k_{cat}/K_m	0.5 ± 0.1	−0.3 ± 0.1	0.2 ± 0.2	0.09 ± 0.02	−0.1 ± 0.2
		AB_NPS	AB_NPB		AB_NP	
Non-patch	k_{cat}	0.10 ± 0.02	0.027 ± 0.004	0.12 ± 0.02	0.17 ± 0.02	0.05 ± 0.04
	K_m	0.27 ± 0.06	0.20 ± 0.04	0.47 ± 0.08	0.5 ± 0.1	0.0 ± 0.2
	k_{cat}/K_m	−0.18 ± 0.04	−0.17 ± 0.04	−0.35 ± 0.06	−0.3 ± 0.1	0.0 ± 0.2

[a] Deviations were defined as 2σ from the mean.

Table 4: Comparison of Free Energy Differences among Chimeras toward Fru 1-P[a]

thermodynamic cycle		$\Delta\Delta G^{\ddagger}$ (kcal/mol) individual chimeras		sum	combined chimeras	ΔG_I (kcal/mol)
		AB_TSP	AB_DSP		AB_P	
Patch	k_{cat}	−0.4 ± 0.08	−0.7 ± 0.1	−1.1 ± 0.1	−0.4 ± 0.1	0.7 ± 0.2
	K_m	0.9 ± 0.2	0.9 ± 0.2	1.8 ± 0.2	1.5 ± 0.4	−0.3 ± 0.4
	k_{cat}/K_m	−1.3 ± 0.4	−1.6 ± 0.4	−2.9 ± 0.6	−1.9 ± 0.6	1.0 ± 0.8
		AB_P	AB_NP		AB_All	
All	k_{cat}	−0.4 ± 0.1	−0.5 ± 0.1	−1.0 ± 0.1	−0.5 ± 0.1	0.5 ± 0.2
	K_m	1.5 ± 0.4	−0.10 ± 0.02	1.4 ± 0.4	1.6 ± 0.4	0.3 ± 0.4
	k_{cat}/K_m	−1.9 ± 0.6	−0.5 ± 0.1	−2.3 ± 0.6	−2.1 ± 0.6	0.2 ± 0.8
		AB_NPS	AB_NPB		AB_NP	
Non-patch	k_{cat}	−0.5 ± 0.1	−0.7 ± 0.1	−1.3 ± 0.2	−0.5 ± 0.1	0.7 ± 0.2
	K_m	−0.10 ± 0.02	−0.45 ± 0.06	−0.54 ± 0.06	−0.1 ± 0.02	0.45 ± 0.06
	k_{cat}/K_m	−0.5 ± 0.1	−0.28 ± 0.06	−0.7 ± 0.1	−0.5 ± 0.1	0.3 ± 0.2

[a] Deviations were defined as 2σ from the mean.

the separate patches, AB_TSP and AB_DSP, was compared to the free energy of swapping of both patches (AB_P) (Figure 3A). Second, the change in free energy associated with separating patch (AB_P) and nonpatch (AB_NP) residues was compared to those produced by swapping all ISRs (AB_All) (Figure 3B). Finally, the free energy associated with separating the nonpatch ISRs into surface (AB_NPS) and buried (AB_NPB) residues was compared to the free energy of swapping of all nonpatch (AB_NP) residues (Figure 3C).

The change in transition-state stabilization energy associated with each set of substitutions was calculated from the kinetic parameters k_{cat} and K_m using eq 1 (*37*, *38*):

$$\Delta\Delta G_T^{\ddagger} = -RT \ln \frac{(k_{cat}/K_m)_{mutant}}{(k_{cat}/K_m)_{wild\ type}} \quad (1)$$

where $\Delta\Delta G_T^{\ddagger}$ is the transition-state stabilization energy or change in free energy to reach the transition-state complex from free enzyme and substrate, R is the gas constant, and T is the absolute temperature. The sum of the changes in free energy for the two single sets of substitutions is related to the change in free energy of the double sets of substitutions by eq 2:

$$\Delta\Delta G_{(X,Y)}^{\ddagger} = \Delta\Delta G_{(X)}^{\ddagger} + \Delta\Delta G_{(Y)}^{\ddagger} + \Delta G_I \quad (2)$$

where $\Delta\Delta G_{(X,Y)}^{\ddagger}$ is the difference in free energy between the wild type and the chimera with the double set of substitutions, $\Delta\Delta G_{(X)}^{\ddagger}$ and $\Delta\Delta G_{(Y)}^{\ddagger}$ are the differences in free energy between the wild type and the two chimeras with a single set of substitutions, and ΔG_I, or coupling energy, is the interaction energy between substitution sites (*38*, *39*). If $\Delta G_I \approx 0$, then the interactions between the sets of ISRs are additive, thus indicating that the ISRs have independent effects. If $\Delta G_I \neq 0$, then the effects are nonadditive, indicating that one set of ISRs is affected by the other set of ISRs. Negative ΔG_I values represent a positive coupling interaction that enhances the kinetic parameter measured, while positive ΔG_I values represent coupling interactions that reduce this parameter (*40*). This analysis was repeated with k_{cat} and again with K_m, substituting each for k_{cat}/K_m in eq 1.

The ΔG_I values calculated for both Fru 1,6-P_2 and Fru 1-P using the three thermodynamic cycles are listed in Tables 3 and 4, respectively. For the thermodynamic cycle "Patch", there was a non-zero ΔG_I for the kinetic parameter k_{cat}/K_m toward Fru 1,6-P_2 (−0.7 kcal/mol). As described above, the negative ΔG_I indicated coupling energy that enhances the kinetic parameter k_{cat}/K_m. This cooperativity was largely associated with the rate-limiting step, k_{cat} (−0.6 kcal/mol). The same analysis using Fru 1-P demonstrated a similar cooperative effect associated with k_{cat}/K_m (ΔG_I = 1.0 kcal/mol). However, the change in sign indicated a negative cooperativity between these two patches for this substrate. Again, as it was for Fru 1,6-P_2, this cooperativity was largely due to an effect on k_{cat} (0.7 kcal/mol).

On the other hand, for the thermodynamic cycles "All" and "Non-patch", the change in free energies associated with each kinetic parameter for Fru 1,6-P_2 was additive ($\Delta G_I \approx 0$). However, the coupling energy for Fru 1-P indicated a small but significant coupling energy between nonpatch surface and nonpatch buried residues associated with k_{cat}/K_m ($\Delta G_I = 0.3$ kcal/mol). This was the net effect of two larger but opposing changes on k_{cat} ($\Delta G_I = 0.7$ kcal/mol) and K_m ($\Delta G_I = 0.45$ kcal/mol). Of the seven nonpatch surface and nonpatch buried residues, five are aldolase B ISRs, suggesting that the coupling interaction between these residues is conserved mainly in aldolase B. It must be noted that this analysis is based on the assumption that the rate-limiting step (product release) for the chimeras has not changed such that K_m has the same definition for all enzymes. Moreover, the pseudo-second-order rate constants, k_{cat}/K_m, are comparable, and it is in this constant that the important distinctions lie.

Involvement of the Flexible C-Terminus. Coupling interactions between sets of ISRs acting at a distance affect substrate specificity. As details of these interactions are unknown, we hypothesized that the flexible C-terminus of aldolase, which is part of the TSP, is a potential "bridge" for mediating these interactions. This is based on X-ray crystallographic data in which disorder (*19*, *24*, *41*) or multiple conformations (*23*, *42*−*44*) of the 18−20 C-terminal residues (CTR) indicate flexibility. Moreover, removal of residues from the CTR of aldolase A disrupts Fru 1,6-P_2 turnover with limited effects on Fru 1-P turnover (*21*, *45*, *46*).

To test this model, a C-terminal mutant of aldolase was generated and the steady-state kinetic parameters were determined. For this variant, the entire CTR was deleted, to make Ald337 (Figure 2), which exhibited a 30−100-fold decrease in k_{cat} compared to that of the wild type for both substrates (Table 2). However, the K_m values were affected in opposite directions; toward Fru 1,6-P_2, the K_m value increased 20-fold, whereas toward Fru 1-P, the K_m decreased 20-fold. Thus, this distinction highlights the importance of the CTR in differential effects on substrate binding and intermediate steps in the catalytic cycle (K_m), and in substrate-specific rate-limiting steps (k_{cat}), likely involving conformational changes. This conclusion was reinforced by comparison to an enzyme that added back the CTR, but included all the ISRs from the TSP of aldolase B (AB_TSP). The turnover number for both Fru 1,6-P_2 and Fru 1-P cleavage was restored to the values for aldolase B (Table 2), yet the values for K_m remained more like that of aldolase A. Thus, the inclusion of the CTR alone is not sufficient to confer the k_{cat} values of aldolase B, and the CTR, while required for full activity toward both substrates, may behave differently upon the binding of each.

Evidence for Mobility of the α-Helical Cluster. The thermodynamic analyses of the kinetic behavior pinpointed the involvement of both the TSP and DSP regions of aldolase. ISRs that comprise the TSP and DSP are generally located on opposite faces of a previously unappreciated cluster of α-helices (Figure 4). The first and last helices off the α/β-barrel (α2 and α13) along with three other nonbarrel helices (α3, α4, and α14) form the five-helix cluster. One mechanism explaining the cooperativity in determination of aldolase substrate specificity may involve conformational changes of these helices during catalysis.

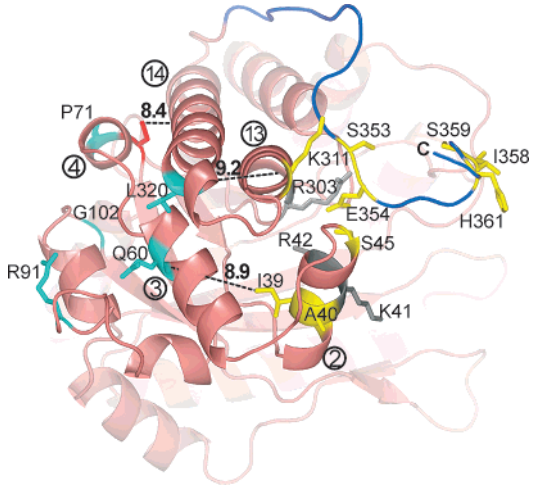

FIGURE 4: Ribbon diagram of aldolase depicting a five-helix cluster. The five helices in the cluster involved in determination of substrate specificity are numbered (circled). The ISRs in the TSP (yellow) and the DSP (cyan) are labeled and depicted as sticks. The monomer is oriented with the active site cleft facing to the right and in the plane of the paper. The distances (angstroms) between near ISRs in the two patches are indicated in addition to the distance between Cys72 and Cys338 (red sticks). Residues involved in binding the C6-phosphate, Lys41, Arg42, and Arg303 (*57*) are depicted as gray sticks, and the Cα backbone of the CTR is colored blue. This figure was created using PDB entry 1ADO and PyMOL version 0.97 (*58*).

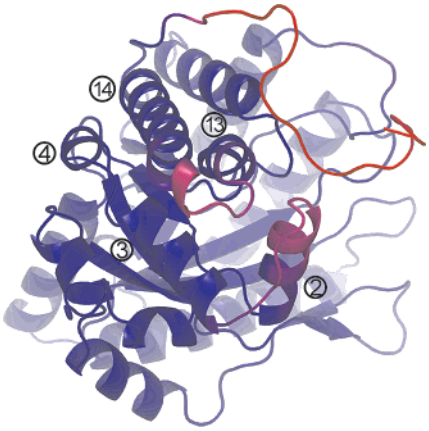

FIGURE 5: Ribbon diagram of aldolase colored by *B*-factor. The five helices in the excursion involved in determination of substrate specificity are numbered (circled). The monomer is oriented with the active site cleft facing to the right and in the plane of the paper. The Cα backbone is colored by increasing *B*-factor from blue (minimum value of 35 $Å^2$) to red (maximum value of 80 $Å^2$). This figure was created using chain A from PDB entry 1ADO and PyMOL version 0.97 (*58*). Other structures in the Protein Data Bank produced a similar result.

Two analyses were preformed to test the model in which the α-helical cluster exhibits substrate-dependent conformational flexibility. The first was an analysis of *B*-factors in the region of the α-helical cluster (Figure 5). Indeed, parts of helices α2, α13, and α14 exhibit elevated values relative to the average *B*-factor of the structure. However, interpretation of mobility from X-ray crystallographic data is not definitive. A direct analysis was performed that derives from the well-known effect of oxidation on aldolase activity (*34*, *47*). Oxidation of surface cysteine residues on aldolase can be protected against loss of activity to different extents by different substrates (*34*). It is thought that the site of oxidation is probably due to the proximal residues Cys72 and Cys338,

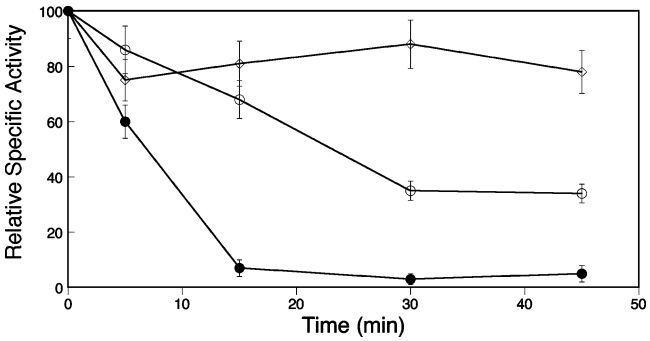

FIGURE 6: Rates of inactivation by oxidation of Cys72 and Cys338 in the presence of substrates. Aldolases with two reactive surface Cys residues (gBi) were incubated in the presence of cupric phenanthroline with or without (●) substrates Fru 1,6-P_2 (◇) or Fru 1-P (○). Activity was measured and normalized to the activity at time zero (9.3−12.8 units/mg). Errors were determined for each experiment, which was repeated three times.

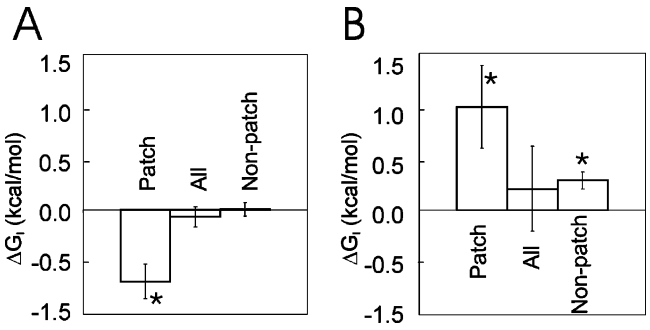

FIGURE 7: Coupling energy associated with k_{cat}/K_m for both substrates in all three thermodynamic cycles. The ΔG_I values (kilocalories per mole) for k_{cat}/K_m toward Fru 1,6-P_2 (A) and Fru 1-P (B) were plotted for the indicated thermodynamic cycles. Asterisks indicate significant nonadditivity of ΔG_I values different from zero by Student's *t*-test ($p < 0.001$).

which are in helices α4 and α14 of the α-helical cluster (see Figure 4). A construct was made that removed the two other reactive cysteine groups and left only Cys72 and Cys338. This construct, gBi, was purified, characterized, and shown to possess kinetic values similar to those of wild-type aldolase A (k_{cat} was 14 s^{-1} and K_m toward Fru 1,6-P_2 was 8.6 μM). This aldolase variant was used to test if oxidation of these Cys residues in the α-helical cluster would show different rates of activity loss due to oxidation in the presence of Fru 1,6-P_2 versus Fru 1-P. When substrates were used at the same concentrations (relative to K_m), Fru 1,6-P_2 exhibited a much slower loss of activity compared to Fru 1-P, which was itself slower relative to enzyme without any substrate (Figure 6). That this effect was due to oxidation at these two Cys residues was shown by the lack of any substrate-dependent loss of activity in the aldolase variant, gTet, which does not possess any surface Cys residues (*31*), and in the loss of DTNB reactivity at the end of the oxidation reaction, which confirmed loss of available thiols in gBi (data not shown). This result is a clear and direct demonstration that the conformation of the helixes containing these two proximal Cys residues in the α-helical cluster is different depending on the substrate present.

DISCUSSION

Recently, it has been proposed that enzyme dynamics is a necessary feature of enzyme catalysis and that structural flexibility dictates the rate of enzyme-catalyzed reactions (*1*, *12*). Thus, identifying what part of an enzyme moves and the consequences of these movements is critical for understanding enzyme kinetics and function. Crystal structures at various stages of catalysis are often used to identify the result of structural movements. For example, crystal structures of DHFR reveal a flexible loop that lies directly over the active site. Movement of the loop causes alterations of the architecture of the active site (*8*). Alternatively, direct visualization of structural movements is possible via NMR (*48*, *49*). Recently, direct observation of motion has been made for T7 DNA polymerase using a conformation sensitive fluorophore to show that discrimination between correct and incorrect nucleotides depends on substrate-induced structural alignment or misalignment of catalytic residues (*13*).

The first evidence for conformational flexibility in aldolase came from studies measuring the accessibility of a surface cysteine in aldolase A, which links conformational flexibility with substrate turnover (*47*). In these studies, the degree of modification of Cys239 (a residue outside the active site) varied depending on the different substrates present; however, these studies did not identify the elements that were moving, or how the movements might differ for different substrates. In attempts to define the important regions as the source of substrate specificity between aldolase isozymes, others have swapped relatively large sections of the primary sequence between isozymes (*50*−*54*). Not surprisingly, the results suggested a role for the CTR in catalysis; however, the minimal set of residues involved in conferring substrate preferences was not identified. Using a more comprehensive approach, a set of residues (ISRs) conserved within and unique to each isozyme that plays a role in specificity among isozymes was defined (*25*). Given the clustering of these residues into discrete patches outside the active site (>8 Å from any catalytic residue), and knowing that they must be involved in distinguishing isozyme specificity, we asked the question of how or if they cooperate in this task using thermodynamic cycles.

Cooperation was directly assessed by interchanging ISR patches between aldolase A and B. Thermodynamic analysis of the kinetic parameters assessed coupling interactions between the various patches of ISRs (Figure 3). The coupling energy between the TSP and DSP revealed that they function cooperatively in analysis of k_{cat}/K_m. The positive cooperative effect toward Fru 1,6-P_2 (negative ΔG_I) was the opposite of the effect observed for cleavage of Fru 1-P (positive ΔG_I). This distinction is illustrated by plotting the coupling energy associated with k_{cat}/K_m for all three thermodynamic cycles toward both substrates (Figure 7). This difference in coupling energy between the two substrates for the two conserved surface patches (TSP and DSP) is consistent with a model that defines the roles of these patches in conferring substrate specificity of aldolase A. These residues work in a cooperative way to enhance k_{cat} for Fru 1,6-P_2 cleavage and work in a negative fashion for Fru 1-P cleavage.

The energetic difference between the two wild-type isozymes for the two substrates can be calculated by substituting the k_{cat}/K_m ratio of Fru 1,6-P_2 to Fru 1-P for each isozyme into eq 1. The resulting value of 2.5 kcal/mol is the quantitative description of the substrate specificity difference between isozymes. Thus, the value of 1.7 kcal/mol measured for the difference in the cooperative effect

(ΔG_I) between the two ISR patches (Figure 7) accounts for ~70% (1.7/2.5) of the total energy difference between the ratio of specificities toward the substrates between aldolase A and B and is therefore likely the major source of the distinction between the two substrates. These energy values are similar in magnitude to those previously determined for the contribution of conformational coupling to single steps in catalysis. For example, ΔG_I values from nonadditivity among sets of single-, double-, and quadruple-substitution mutants of DHFR have been measured for the hydride transfer rates (1.7−2.1 kcal/mol) and cofactor binding (0.6−1.7 kcal/mol) (*9*, *55*).

Mapping the TSP and DSP on the structure of aldolase A revealed that the closest residues were more than 8 Å apart (see Figure 4). The thermodynamic analyses and substrate protection against oxidation support a model that involves differential conformational changes of these regions. In this model, movement of the flexible CTR is coupled to transient structural changes in the ISRs of the TSP and the DSP. Structural changes induced by each substrate would influence the location of the flexible CTR, which is structurally connected to this cluster at α14. Importantly, α2 includes Lys41 and Arg42, which comprise part of the C6-phosphate binding site (*56*, *57*). Thus, a structural connection exists between a substrate binding site and the ISRs involved in determining substrate specificity.

Such a model for conformational flexibility not only fits the data presented herein but also provides an explanation for previously unexplained observations for aldolase. The previous observation is that Cys72 and Cys338, which are located 8.4 Å apart (*42*), can form an inactivating disulfide bond (*34*). Due to the distance separating them, conformational changes would be necessary to allow bond formation. Our analysis reveals that these two cysteines are part of the five-helix cluster. Cys338 is located at the end of α14 and Cys72 located after the end of α4 (see Figure 4). The formation of a disulfide bond between Cys72 and Cys338 could be the result of a trapped transient conformational change in the five-helix cluster. In the model, rigidification of this region by disulfide bond formation would severely impact catalysis. Second, studies measuring the accessibility of surface cysteines in aldolase A have linked conformational changes to catalysis (*47*). In these studies, the accessibility of Cys239 was monitored by chemical modification in the presence of the substrates. Cys239 was less accessible to protein modification in the presence of Fru 1,6-P_2 than in the presence of Fru 1-P. The distance from Cys239 to the active site indicated that long-range conformational changes are coupled to cleavage of specific substrates. Thus, the authors conclude "substrate induced conformational changes in aldolase are syncatalytic in nature" (*47*).

The aldolase isozymes have evolved to perform functions that are physiologically relevant to the tissue in which they are expressed. Results given here define the differences between substrates in terms of conformational coupling between residues in the TSP and those distant from the active site in the DSP as well as the CTR. The two patches comprise a newly identified structural element composed of five helices. These results explain kinetic distinctions among isozymes that have identical active sites. Thus, this study shows the value of thermodynamic analysis of modified enzymes for revealing cooperative interactions linked to substrate specificity. Use of this method is the first of what will likely be many demonstrating the role of enzyme dynamics in determining substrate specificity.

ACKNOWLEDGMENT

We thank Dr. Nicholas Silvaggi for critical review of the manuscript.

SUPPORTING INFORMATION AVAILABLE

A complete list of the oligonucleotides used for construction of the aldolase chimeras. This material is available free of charge via the Internet at http://pubs.acs.org.

REFERENCES

1. Hammes-Schiffer, S., and Benkovic, S. J. (2006) Relating protein motion to catalysis, *Annu. Rev. Biochem. 75*, 519−541.
2. Schnell, J. R., Dyson, H. J., and Wright, P. E. (2004) Structure, dynamics, and catalytic function of dihydrofolate reductase, *Annu. Rev. Biophys. Biomol. Struct. 33*, 119−140.
3. Wand, A. J. (2001) Dynamic activation of protein function: A view emerging from NMR spectroscopy, *Nat. Struct. Biol. 8*, 926−931.
4. Gunasekaran, K., Ma, B., and Nussinov, R. (2004) Is allostery an intrinsic property of all dynamic proteins, *Proteins 57*, 433−443.
5. Cooper, A., and Dryden, D. T. (1984) Allostery without conformational change. A plausible model, *Eur. Biophys. J. 11*, 103−109.
6. Lockless, S. W., and Ranganathan, R. (1999) Evolutionarily conserved pathways of energetic connectivity in protein families, *Science 286*, 295−299.
7. Labeikovsky, W., Eisenmesser, E. Z., Bosco, D. A., and Kern, D. (2007) Structure and Dynamics of Pin1 During Catalysis by NMR, *J. Mol. Biol. 367*, 1370−1381.
8. Miller, G. P., and Benkovic, S. J. (1998) Stretching exercises: Flexibility in dihydrofolate reductase catalysis, *Chem. Biol. 5*, R105−R113.
9. Huang, Z., Wagner, C. R., and Benkovic, S. J. (1994) Nonadditivity of mutational effects at the folate binding site of *Escherichia coli* dihydrofolate reductase, *Biochemistry 33*, 11576−11585.
10. Liang, Z. X., Tsigos, I., Lee, T., Bouriotis, V., Resing, K. A., Ahn, N. G., and Klinman, J. P. (2004) Evidence for increased local flexibility in psychrophilic alcohol dehydrogenase relative to its thermophilic homologue, *Biochemistry 43*, 14676−14683.
11. Liang, Z. X., Lee, T., Resing, K. A., Ahn, N. G., and Klinman, J. P. (2004) Thermal-activated protein mobility and its correlation with catalysis in thermophilic alcohol dehydrogenase, *Proc. Natl. Acad. Sci. U.S.A. 101*, 9556−9561.
12. Liang, Z. X., and Klinman, J. P. (2004) Structural bases of hydrogen tunneling in enzymes: Progress and puzzles, *Curr. Opin. Struct. Biol. 14*, 648−655.
13. Tsai, Y. C., and Johnson, K. A. (2006) A new paradigm for DNA polymerase specificity, *Biochemistry 45*, 9675−9687.
14. Horecker, B. L., Tsolas, O., and Lai, C. Y. (1975) Aldolases, in *The Enzymes* (Boyer, P. D., Ed.) pp 213−258, Academic Press, New York.
15. Lebherz, H. G., and Rutter, W. J. (1969) Distribution of fructose diphosphate aldolase variants in biological systems, *Biochemistry 8*, 109−121.
16. Kusakabe, T., Motoki, K., and Hori, K. (1994) Human aldolase C: Characterization of the recombinant enzyme expressed in *Escherichia coli*, *J. Biochem. 115*, 1172−1177.
17. Penhoet, E. E., and Rutter, W. J. (1971) Catalytic and immunochemical properties of homomeric and heteromeric combinations of aldolase subunits, *J. Biol. Chem. 246*, 318−323.
18. Hers, H.-G. (1957) *Le Métabolisme du Fructose*, Editions Arsica, Brussels.
19. Choi, K. H., Shi, J., Hopkins, C. E., Tolan, D. R., and Allen, K. N. (2001) Snapshots of catalysis: The structure of fructose-1,6-(bis)phosphate aldolase covalently bound to the substrate dihydroxyacetone phosphate, *Biochemistry 40*, 13868−13875.
20. Rose, I. A., Warms, J. V. B., and Kuo, D. J. (1987) Concentration and partitioning of intermediates in the fructose bisphosphate aldolase reaction. Comparison of the muscle and liver enzymes, *J. Biol. Chem. 262*, 692−701.

21. Rose, I. A., O'Connell, E. L., and Mehler, A. H. (1965) Mechanism of the aldolase reaction, *J. Biol. Chem. 240*, 1758−1765.
22. Gamblin, S. J., Davies, G. J., Grimes, J. M., Jackson, R. M., Littlechild, J. A., and Watson, H. C. (1991) Activity and specificity of human aldolases, *J. Mol. Biol. 219*, 573−576.
23. Dalby, A., Tolan, D. R., and Littlechild, J. A. (2001) Crystal structure of human liver fructose 1,6-bisphosphate aldolase, *Acta Crystallogr. D57*, 1526−1533.
24. Arakaki, T. L., Pezza, J. A., Cronin, M. A., Hopkins, C. E., Zimmer, D. B., Tolan, D. R., and Allen, K. N. (2004) Structure of human brain fructose 1,6-bisphosphate aldolase: Linking isozyme structure with function, *Protein Sci. 13*, 3077−3084.
25. Pezza, J. A., Choi, K. H., Berardini, T. Z., Beernink, P. T., Allen, K. N., and Tolan, D. R. (2003) Spatial clustering of isozyme-specific residues reveals unlikely determinants of isozyme specificity in fructose 1,6-bisphosphate aldolase, *J. Biol. Chem. 278*, 17307−17313.
26. Ackers, G. K., Doyle, M. L., Myers, D., and Daugherty, M. A. (1992) Molecular code for cooperativity in hemoglobin, *Science 255*, 54−63.
27. Cronin, C. N., and Kirsch, J. F. (1988) Role of arginine-292 in the substrate specificity of aspartate aminotransferase as examined by site-directed mutagenesis, *Biochemistry 27*, 4572−4579.
28. Ho, S., Hunt, H., Horton, R., Pullen, J., and Pease, L. (1989) Site-directed mutagenesis by overlapping extension using the polymerase chain reaction, *Gene 77*, 51−59.
29. Morris, A. J., and Tolan, D. R. (1993) Site-directed mutagenesis identifies aspartate 33 as a previously unidentified critical residue in the catalytic mechanism of rabbit aldolase A, *J. Biol. Chem. 268*, 1095−1100.
30. Beernink, P. T., and Tolan, D. R. (1992) Construction of a high-copy "ATG vector" for expression in *Escherichia coli*, *Protein Expression Purif. 3*, 332−336.
31. Hopkins, C. E., O'Conner, P. B., Allen, K. N., Costello, C. E., and Tolan, D. R. (2002) Chemical-modification rescue assessed by mass spectrometry demonstrates γ-thia-lysine yields the same activity as lysine in aldolase, *Protein Sci. 11*, 1591−1599.
32. Pezza, J. A., Allen, K. N., and Tolan, D. R. (2004) Intein-mediated purification of a recombinantly expressed peptide, *Chem. Commun.*, 2412−2413.
33. Racker, E. (1947) Spectrophotometric measurement of hexokinase and phosphohexokinase activity, *J. Biol. Chem. 167*, 843−854.
34. Kobashi, K., and Horecker, B. L. (1967) Reversible inactivation of rabbit muscle aldolase by *o*-phenanthroline, *Arch. Biochem. Biophys. 121*, 178−186.
35. Connolly, M. L. (1983) Analytical molecular surface calculation, *J. Appl. Crystallogr. 16*, 548−558.
36. Morris, A. J., and Tolan, D. R. (1994) Lysine-146 of rabbit muscle aldolase is essential for cleavage and condensation of the C3−C4 bond of fructose 1,6-bis(phosphate), *Biochemistry 33*, 12291−12297.
37. Wilkinson, A. J., Fersht, A. R., Blow, D. M., and Winter, G. (1983) Site-directed mutagenesis as a probe of enzyme structure and catalysis: Tyrosyl-tRNA synthetase cysteine-35 to glycine-35 mutation, *Biochemistry 22*, 3581−3586.
38. Carter, P. J., Winter, G., Wilkinson, A. J., and Fersht, A. R. (1984) The use of double mutants to detect structural changes in the active site of the tyrosyl-tRNA synthetase (*Bacillus stearothermophilus*), *Cell 38*, 835−840.
39. Ackers, G. K., and Smith, F. R. (1985) Effects of site-specific amino acid modification on protein interactions and biological function, *Annu. Rev. Biochem. 54*, 597−629.
40. Wells, J. A. (1990) Additivity of mutational effects in proteins, *Biochemistry 29*, 8509−8517.
41. Sygusch, J., Beaudry, D., and Allaire, M. (1987) Molecular architecture of rabbit skeletal muscle aldolase at 2.7-Å resolution, *Proc. Natl. Acad. Sci. U.S.A. 84*, 7846−7850.
42. Blom, N., and Sygusch, J. (1997) Product binding and role of the C-terminal region in class I D-fructose 1,6-bisphosphate aldolase, *Nat. Struct. Biol. 4*, 36−39.
43. St-Jean, M., Lafrance-Vanasse, J., Liotard, B., and Sygusch, J. (2005) High resolution reaction intermediates of rabbit muscle fructose-1,6-bisphosphate aldolase: Substrate cleavage and induced fit, *J. Biol. Chem. 280*, 27262−27270.
44. Maurady, A., Zdanov, A., de Moissac, D., Beaudry, D., and Sygusch, J. (2002) A conserved glutamate residue exhibits multifunctional catalytic roles in D-fructose-1,6-bisphosphate aldolases, *J. Biol. Chem. 277*, 9474−9483.
45. Rutter, W. J., Richards, O. C., and Woodfin, B. M. (1961) Comparative studies of liver and muscle aldolase. I. Effect of carboxypeptidase on catalytic activity, *J. Biol. Chem. 236*, 3193−3197.
46. Dreschler, E. R., Boyer, P. D., and Kowalsky, A. G. (1959) The catalytic activity of carboxypeptidase-degraded aldolase, *J. Biol. Chem. 234*, 2627−2634.
47. Heyduk, T., Michalczyk, R., and Kochman, M. (1991) Long-range effects and conformational flexibility of aldolase, *J. Biol. Chem. 266*, 15650−15655.
48. Kay, L. E. (1998) Protein dynamics from NMR, *Nat. Struct. Biol. 5* (Suppl.), 513−517.
49. Boehr, D. D., Dyson, H. J., and Wright, P. E. (2006) An NMR perspective on enzyme dynamics, *Chem. Rev. 106*, 3055−3079.
50. Berthiaume, L., Tolan, D. R., and Sygusch, J. (1993) Differential usage of the carboxyl-terminal region among aldolase isozymes, *J. Biol. Chem. 268*, 10826−10835.
51. Motoki, K., Kitajima, Y., and Hori, K. (1993) Isozyme-specific modules on human aldolase A molecule: Isozyme group-specific sequences 1 and 4 are required for showing characteristics as aldolase A, *J. Biol. Chem. 268*, 1677−1683.
52. Kitajima, Y., Takasaki, Y., Takahashi, I., and Hori, K. (1990) Construction and properties of active chimeric enzymes between human aldolases A and B. Analysis of molecular regions which determine isozyme-specific functions, *J. Biol. Chem. 265*, 17493−17498.
53. Takasaki, Y., Kitajima, Y., Takahashi, I., Sakakibara, M., Mukai, T., and Hori, K. (1990) Structural studies on aldolase isozymes through protein engineering, *Prog. Clin. Biol. Res. 344*, 935−953.
54. Takasaki, Y., and Hori, K. (1992) Studies on chimeric fusion proteins of human aldolase isozymes A and B, *Protein Eng. 5*, 101−104.
55. Rajagopalan, P. T., Lutz, S., and Benkovic, S. J. (2002) Coupling interactions of distal residues enhance dihydrofolate reductase catalysis: Mutational effects on hydride transfer rates, *Biochemistry 41*, 12618−12628.
56. Dalby, A., Dauter, Z., and Littlechild, J. A. (1999) Crystal structure of human muscle aldolase complexed with fructose 1,6-bisphosphate: Mechanistic implications, *Protein Sci. 8*, 291−297.
57. Choi, K. H., Mazurkie, A. S., Morris, A. J., Utheza, D., Tolan, D. R., and Allen, K. N. (1999) Structure of a fructose-1,6-bis-(phosphate) aldolase liganded to its natural substrate in a cleavage-defective mutant at 2.3 Å, *Biochemistry 38*, 12655−12664.
58. DeLano, W. L. (2002) *PyMOL*, version 0.97, DeLano Scientific, San Carlos, CA.

BI700713S